FINAL REVISED VERSION OF THE ARTICLE

Crystal Growth, Optical and Spectroscopic Characterization of the Ytterbium-doped Laser Molybdate Yb-$Li_3Gd_3Ba_2(MoO_4)_8$

Chem. Mater. 2008, 20, 3884–3891

*Alberto García-Cortés, Concepción Cascales**

Instituto de Ciencia de Materiales de Madrid CSIC, c/ Sor Juana Inés de la Cruz, 3, Cantoblanco, 28049 Madrid, Spain.

For article requests, please contact C. Cascales at ccascales@icmm.csic.es

Graphic Abstract for the Table of Contents

A. García-Cortés and C. Cascales*

Crystal Growth, Optical and Spectroscopic Characterization of the Ytterbium-doped Laser Molybdate Yb-$Li_3Gd_3Ba_2(MoO_4)_8$

The monoclinic *C*2/*c* Yb^{3+}-doped $Li_3Gd_3Ba_2(MoO_4)_8$ laser crystal has been successfully grown with optical quality by the TSSG method. The crystal structure has a single 8*f* site occupied simultaneously by Gd^{3+} (72.5%), Yb^{3+} (6%) and Li^+ (21.5%). This leads to a locally disordered environment around Yb^{3+} ions, which generates the observed inhomogeneous broadening of the spectral features. Crystal field splittings for $^2F_{7/2}$ and $^2F_{5/2}$ Yb^{3+} manifolds have been determined.

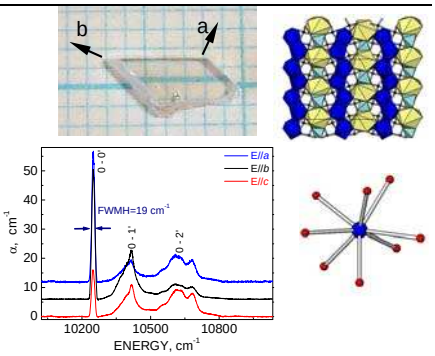

ABSTRACT. Because of the existence of a phase transition at temperature lower than the melting point, Yb-doped $Li_3Gd_3Ba_2(MoO_4)_8$ was grown by the Top Seeded Solution Growth slow cooling method using $Li_2Mo_2O_7$ as flux. At room temperature the crystal possesses the monoclinic symmetry of the space group *C*2/*c* (No. 15), with lattice parameters a = 5.2355(3) Å, b = 12.7396(8) Å, c = 19.1626(11) Å, β = 91.170(1)º, and only one 8*f* crystal site for Yb^{3+}, which is shared with Li^+ and Gd^{3+} cations. The information provided by the low temperature (6K) spectroscopy indicates crystal field splittings of 0, 223, 353 and 460 cm^{-1}, and 10248, 10413 and 10634 cm^{-1}, for $^2F_{7/2}$ and $^2F_{5/2}$ Yb^{3+} manifolds, respectively, and the spectral broadening observed is attributed to locally disordered environments around 8*f* Yb^{3+} centers. Ultraviolet and infrared optical absorption edges of this biaxial laser crystal have been also characterized.

KEYWORDS: Crystal growth; Disordered structures; Yb-doped solid-state lasers; Crystal field. Energy levels.

Introduction

Diode-pumped solid state lasers based on Yb^{3+}-doped crystals are interesting alternatives to those based on Nd^{3+} for cw tunable and ultrashort pulse[1,2] or high power laser applications[3,4] in the wavelength range near 1 μm. Stronger interactions of Yb^{3+} electronic states with lattice vibrations,[5] which lead to large homogeneous spectral broadening and to larger laser gain bandwidths, and smaller Stokes shifts with regards to Nd^{3+} counterparts are accounting for such functionalities and recognition of Yb-based lasers. The main disadvantage of Yb^{3+} lasers crystals is associated to the quite high threshold pump power required by the quasi-three-level room temperature operating laser scheme, but it can be overcame in crystal hosts producing adequately large ground state $^2F_{7/2}$ splitting through strong crystal field effects. Since the relation between the spectroscopic characteristics and laser properties is particularly dependent on structural characteristics related to symmetry and bonding of the Yb^{3+} site in the crystal framework, crystals with short bonding distances and/or largely distorted coordination polyhedra around Yb^{3+} must be selected.[6]

On the other hand, wide tunable and ultrashort pulsed Yb^{3+} laser emission can be expected in multisite hosts, that is, crystals with more than one crystallographic site occupied by Yb^{3+}, being favoured specially by the existence of structural disorder around these sites, as it has been previously demonstrated for $CaGdAlO_4$,[1] $SrY_4(SiO_4)_3O$,[7] and recently for tetragonal double tungstates (DT) and double molybdates (DM) $AT(XO_4)_2$ (A = monovalent Li or Na; T = trivalent Y, Gd, or Lu, X= Mo or W),[2, 8, 9, 10] derived from the total replacement of Ca^{2+} in $CaXO_4$, all of them showing large inhomogeneous broadened spectral bands.

As an alternative to the these DT and DM crystals, the partial substitution of the divalent cation D in the general DXO_4 formula will lead to a number of compounds with more complex compositions, which can offer appropriate sites for Yb^{3+} substitution, and additionally provide multiple distributions of cationic environments around these sites due to the coexistence of mono-, di- and trivalent cations located in them.

Inspecting already known compositions for ternary molybdates [11] with the indicated desirable structural characteristics, $Li_3Gd_3Ba_2(MoO_4)_8$ (hereafter shortly LiGdBaMo) results to be a suitable crystal phase. Its structural description[12] in the monoclinic space group *C*2/*c* (No 15) indicated the existence of two crystal point sites for Gd^{3+}, with very different symmetries, 8*f* and 4*e*. Moreover both sites are shared, the general 8*f* site being simultaneously occupied by Li^+, Gd^{3+} and Ba^{2+}, and the special 4*e* site for Gd^{3+} and Ba^{2+} cations. Around these crystal sites the corresponding $Gd(Yb)1O_8$ and $Gd(Yb)2O_{10}$ polyhedra present extended ranges of Gd(Yb)-O bonding distances, from 2.374 Å to 2.508 Å, and from 2.684 Å to 3.079 Å, respectively. The distortion degree of the last polyhedron, estimated as $\Delta_d = 1/10\Sigma(d_i-d_{aver}/d_{aver})^2$ [ref [13]], is very high, $22.5x10^{-3}$, and it could be indicative of strong crystal field interaction for the 4*e* site, thus yielding large $^2F_{7/2}$ splitting, that along with the expected structural disorder could provide large spectral bandwidths. In fact, Nd^{3+}-doped LiGdBaMo has been reported as a structurally disordered laser crystal,[14] for which continuous and passive Q-switching diode-pumped laser operation has been demosnstrated.[15]

In this paper we presents results on the study the thermal stability of the monoclinic *C*2/*c* phase of LiGdBaMo:Yb, and thus the conditions for the successful growth by the slow cooling Top Seeded Solution Growth (TSSG) method of adequate large crystals for spectroscopic and laser experiments. The crystallographic structure of the grown crystal has been studied by single crystal X-ray diffraction. The transparency range of the crystal and the sequence of Yb^{3+} energy levels determined from low temperature (6 K) polarized optical absorption and photoluminescence spectra, and further assessed with predictive structure-based simulations of crystal field interactions, are also reported.

Experimental techniques

Preparation of Polycrystalline Samples and Crystal Growth

Required stoichiometric amounts of analytical-grade BaO_2, Li_2CO_3, MoO_3, Gd_2O_3 and Yb_2O_3, were used in the synthesis of LiGdBaMo:Yb and $Li_2Mo_2O_7$, the polycrystalline precursor (solute) and the utilized flux, respectively. Lanthanide sesquioxides were 99.99% Alfa Aesar reagents. The preparation

of the solute and flux as well as the Top Seeded Solution crystal Growth (TSSG) slow cooling experiments were made using Pt-crucibles and a vertical tubular furnace with Si_2Mo as heating element. The temperature was set with a resolution better than ± 0.2º C using an Eurotherm 818P temperature controller. To test the purity of crystal phases, standard room temperature X-ray powder diffraction (XRPD) analysis of both synthesized polycrystalline solute and flux were performed with a Bruker AXS D-8 Advance diffractometer, using CuK_α radiation. 2θ scans were made in the angular range of $5º \leq 2\theta \leq 80º$, with $\Delta 2\theta = 0.02º$ steps and a counting time of 2 s per step.

Thermal analyses were made by differential scanning calorimetry (DSC) in a Setaram SetSys Evolution 1700 DTG-DSC system. Amounts of about 50 mg of mixtures of the solute with the flux in several selected ratios were heated and cooled in complete thermal cycles to determine the most adequate composition of the solute-flux mixture to perform the growth process. Furthermore, the thermal stability of the polycrystalline precursor was checked through two complete heating/cooling thermal cycles. Pt crucibles and a constant argon flow were used.

The crystal habit and morphology of grown crystals were simulated with the Donnay-Harker-based SHAPE software.[16]

Single Crystal X-ray Diffraction Analysis

A prismatic colorless suitable single crystal cut from the grown LiGdBaMo:Yb crystal was mounted on a Bruker SMART CCD diffractometer equipped with a normal focus 3 kW sealed tube. Data were collected at room temperature over a hemisphere of the reciprocal space by a combination of three sets of exposures. Each set had a different φ angle for the crystal and each exposure of 20 s covered 0.3º in ω. The crystal to detector distance was 5.01 cm. The unit cell parameters were determined by a least square fit of about 40 reflections with $I > 20\sigma(I)$. Neutral-atom scattering factors for all atoms were used, and anomalous dispersion corrections were applied.[17] The structure was solved by direct methods. Special positions of Li atoms were located in difference Fourier maps. SADABS absorption correction was applied at the end of cycles of the isotropic refinement. Refinement was for full-matrix least squares analysis, with anisotropic thermal parameters for all atoms excepting Li, which was

isotropically refined. The calculations were performed using the SHELXTL program,[18] and the views of the structure were drawn with the ATOMS software.[19]

Spectroscopic Characterization

For optical measurements the crystals were oriented by Laue X-ray diffraction patterns, cut, and polished with diamond paste. Simulations of the Laue patterns were obtained with LAUE.[20]

Optical absorption measurements were made in a Varian spectrophotometer model Cary 5E (λ = 200-3000 nm), and with a Bruker spectrophotometer (model IFS66v/S, λ = 1.3-200 μm). The sample temperature was varied in the 6-300 K range by using a He close-cycle Oxford cryostat equipped with the proper temperature controller. For polarized measurements the sample was inserted between a Glan-Taylor polarizer and a depolarizer sheet. The spectra were measured with the electric field components of the light parallel to each one of the three crystallographic axes, E//*a*, E//*b*, E//*c*. The photoluminescence was excited with a Ti-sapphire laser, dispersed in a SPEX 340-E spectrometer (f = 34 cm) and detected with a 77 K cooled Ge photodiode and a lock-in amplifier.

Results and Discussion

Synthesis and Crystal Growth. A nominal 10 mol% Yb-doping level in LiGdBaMo, comparable to its concentration in previous DT [2,9,10,21,22] and DM,[8,23,24] was chosen. To prepare a suitable polycrystalline precursor, isostructural with the phase previously described,[12] the obtained products of several thermal treatments, from 500 ^{0}C to the melting temperature, with annealing times of 48 h to two weeks, have been monitored by XRPD. A well-crystallized sample with the features of the PDF 77-0830 pattern[25] can be obtained from 550 to 650 ^{0}C, the lower temperatures requiring longer annealing times. It has been observed that XRPD patterns corresponding to samples synthesized at higher temperature show only small changes, see Figure 1, involving slightly different distributions of the intensity *I* of *hkl* peaks, which could be attributed to progressive loss of Li and that would finally yield $Gd_2Ba(MoO_4)_4$:Yb see the simulated XRPD pattern also included in Figure 1. $Gd_2Ba(MoO_4)_4$ has the structure named as $Nd_2Ba(MoO_4)_4$-type, [26] with the monoclinic symmetry of the space group *C*2/*c* and unit cell parameters

a = 5.263 Å, b= 19.33 Å, c =12.677 Å, γ = 91.399 °. [27] The XRDP pattern of the melted at 960 ^{0}C product is similar to the previous ones, and the intensity differences observed in *hkl* peaks with regards to LiGdBaMo:Yb polycrystalline powders synthesized at low temperatures are more likely due to texturing that to presence of $Gd_2Ba(MoO_4)_4$ achieved after a complete loss of Li. The clear distinction between both crystal phases -or the account of any additional overlapped new one-, is not straightforward given the high density of reflections and their match in reason of the closeness between both unit cells parameters. In any case, these results indicate that the searched LiGdBaMo:Yb crystal must be grown at adequately low temperatures to discard any eventual Li volatilisation.

In parallel to XRPD analyses, the thermal stability and possible phase transitions of LiGdBaMo:Yb have been studied by DSC. Figure 2 shows the dependence of the heat flow with the temperature (DSC curves) between 20 and 1150 ^{0}C of the polycrystalline LiGdBaMo:Yb precursor. In the first heating/cooling cycle, at scanning rate 10 ^{0}C min^{-1}, see Figure 2a-1, two endothermic peaks are observed during the heating, with maxima at 680 ^{0}C and 983 ^{0}C. The higher temperature peak corresponds to a solid-liquid transformation, also observed in crystal growth experiments. Upon cooling, the DSC curve shows two exothermic peaks, both sharper than in the heating run, with maxima at 956 ^{0}C and 601 ^{0}C, the first corresponding to the re-solidification of LiGdBaMo:Yb. The temperature of these two exothermic peaks is shifted with regards to the corresponding endothermic ones in the melting, being especially considerable the hysteresis for the observed lower temperature maxima, 79 ^{0}C, see Table 1.

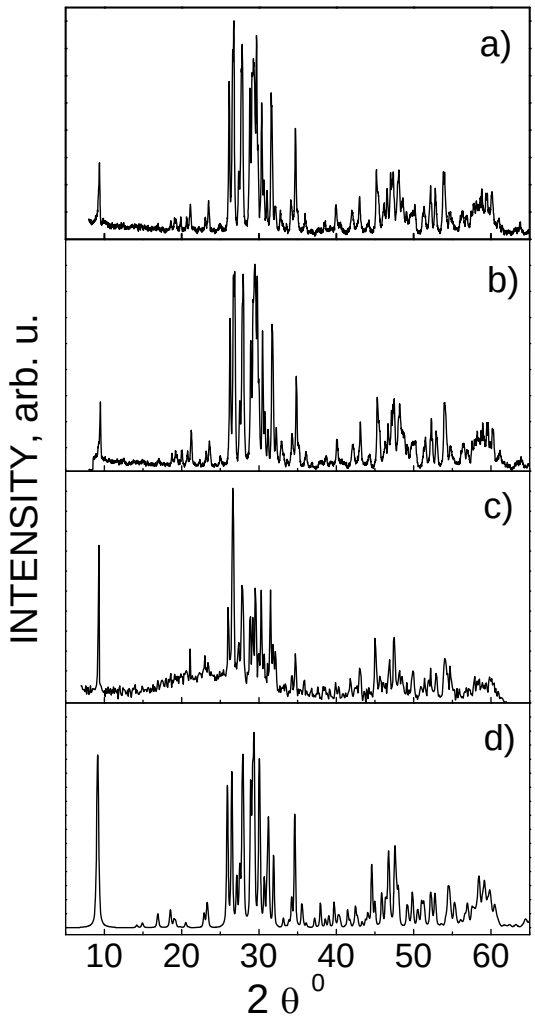

Figure 1. Room temperature X-ray diffraction patterns of a) the LiGdBaMo:Yb polycrystalline precursor synthesized at 600 ^{0}C during two days; b) the same latter sample with an additional annealing at 700 ^{0}C during one day; c) grounded sample from LiGdBaMo:Yb melted at 960 ^{0}C; d) Simulated pattern for $Gd_2Ba(MoO_4)_4$. (CuK_α=1.5406 Å).

The second cycle, Figure 2b, carried out with the resulting material from the fist cycle also at scanning rate 10 ^{0}C min^{-1}, presents a similar pattern, with endothermic peaks at 679 ^{0}C and 983 ^{0}C, and exothermic maxima at 958 ^{0}C and 598 ^{0}C, the most noticeable changes being the rather broadened

endothermic signal corresponding to the melt, and the observed higher entalphy change for the lower temperature phase transition in the heating path, now similar to the corresponding upon cooling, see Table 1

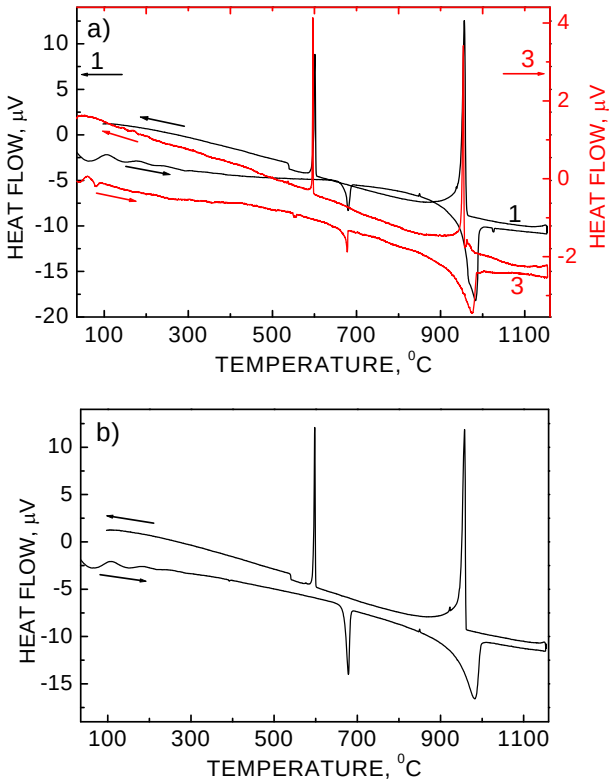

Figure 2. DSC curves of heating/cooling cycles of the LiGdBaMo:Yb polycrystalline precursor: a) At scanning rate 10 ^{0}C.min^{-1} (1, black), and at 3 ^{0}C.min^{-1} (3, red); b) second cycle at 10 ^{0}C.min^{-1}.

Along these two cycles the temperatures of corresponding peaks are the almost the same, and since no appreciable variation of weight has been observed, it is possible to conclude that the existing crystal phases are the same in both cycles. Even if some slight loss of Li can be considered, yielding a Li-deficient LiGdBaMo:Yb composition, the presence of $Gd_2Ba(MoO_4)_4$:Yb as a decomposition product must be discarded, since its melting point is expected to be 50-70 ^{0}C higher than for LiGdBaMo:Yb,[12] and it should be more able to be seen in the second heating cycle. Both stoichiometric ternary LiGdBaMo and double $Gd_2Ba(MoO_4)_4$ molybdate crystals have the same crystal structure, with symmetry *C*2/*c*, and their unit-cell parameters are very close, but the latter has a distinctive congruent

melting,[12] and in fact, $Gd_2Ba(MoO_4)_4$:Yb crystals for laser experiments have been recently grown by the Czochralski method, at 1070 ^{0}C.[28]

Table 1. Characteristics of the thermal behaviour of the LiGdBaMo:Yb polycrystalline precursor

		HEATING			COOLING			
CYCLE	SR [a] (^{0}C.min^{-1})	T_{onset} (^{0}C)	T_{peak} (^{0}C)	ΔH (μV.s/mg)	T_{onset} (^{0}C)	T_{peak} (^{0}C)	ΔH (μV.s/mg)	ΔT (^{0}C)
1[b]	10	673.3	679.8	1.9151	603.8	601.1	-4.9340	79
		951.8	982.9	20.2646	960.9	956.1	-17.9319	27
2[b]	10	668.0	678.7	5.1875	599.8	597.8	-5.1613	81
		932.3	982.5	21.6909	961.3	957.9	-19.8614	25
3[c]	3	672.9	677.9	2.2221	597.4	596.1	-5.2739	82
		948.3	974.9	24.6390	955.9	954.1	-16.0604	21

[a] SR: scanning rate

[b] Consecutively carried out experiments with the same LiGdBaMo:Yb polycrystalline power

[c] Experiment carried out with other amount of LiGdBaMo:Yb polycrystalline powder

The above experimental findings suggest that a reversible first-order phase transformation at the temperature range 600-680 ^{0}C exists for this ternary molybdate. Indeed, the polymorphism is a well-known feature of triple and double molybdates and tungstates.[29,30] However, since no appreciable changes have been detected in XRPD patterns taken for samples annealed for several hours (even days) at temperatures below and above this temperature range, the phase transition does not seem correspond to a change in the crystal symmetry. Results of optical absorption measurements further confirm this point, see the provided Supporting Information. The isosymmetrical phase transition is possibly related to subtle geometrical changes in the framework, as those derived from tilting of the MoO_4 tetrahedra,[31]

Jahn-Teller distortions in LiO_6 octahedra[32] or their combined effects, among others, which could be associated to some charge ordering of Li^+ and Gd^{3+} [33] over the site that they simultaneously occupy.

To check if the hysteresis width of the two peaks depends on the scanning rate, a slower 3 ^{0}C min^{-1} complete cycle was performed with another portion of the same polycrystalline precursor, see the Figure 2a-3 for the DSC curve, and Table 1 for the characteristics of the observed peaks. While the hysteresis for the first peak remains almost the same, some decrease in the melting-point hysteresis width, mainly due to the lessening of the temperature melting on heating, can be detected. Subsequent heating/cooling cycles, or slow scanning rates seem thus diminish the temperature for melting.

The phase transition for LiGdBaMo:Yb prevents its crystal growth by the Czochralski technique. The TSSG slow cooling method and $Li_2Mo_2O_7$ as the flux, with melting point adequately low, have been used to grow these single crystals. Moreover, the use of this flux will compensate any possible volatilisation of Li and Li-deficiency [34] in the grown crystal. The crystallization temperature, that is, the saturation temperature for different mixtures of LiGdBaMo:Yb and $Li_2Mo_2O_7$ has been determined by DSC as the resolidification temperature after melting upon cooling, in each case. The results, the solubility curve for the used flux, can be observed in the Figure 3. A mixture with molar solute/flux ratio of 2.66:97.34, corresponding to 15 wt% of solute and 85 wt% of flux resulted to be the most suitable composition for the crystal growth of LiGdBaMo:Yb crystals. This mixture allows the best control of the crystallization process, see Figure 3, and its melting occurs at a temperature that prevents any undesired phase transformation. For homogenisation, it was kept 20 hours at ≈ 50 ^{0}C above the melting temperature, and then it was decreased to the crystallization point. The cooling interval was 11 ^{0}C, and the cooling rate 0.08 ^{0}C/h. A Pt wire was used as seed, and its rotation speed was 12 rpm. Transparent colourless crystals, with rhombic prismatic shape, as this shown in Figure 4a, were obtained. Other attempts to grow crystals from mixtures with larger concentration of the solute, and thus higher temperature of melting, were unsuccessful due to the cracking of the crystal upon cooling, when the temperature of the phase transition was reached.

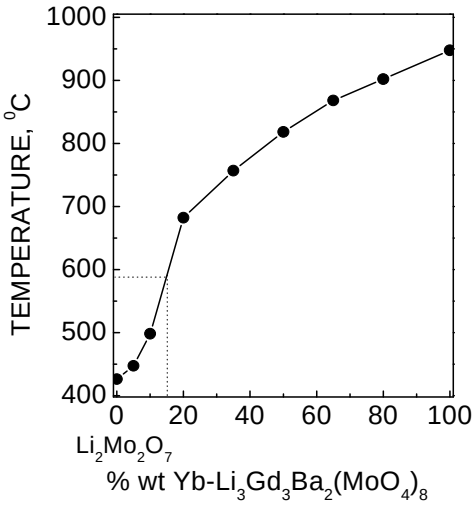

Figure 3. Solubility curve of LiGdBaMo:Yb in the $Li_2Mo_2O_7$ flux.

Figure 4b shows morphological schemes of the grown crystal indicating its faces and crystal axes, simulated according the Donnay-Harker law[35] with the SHAPE software.[16] Required cell parameters and space group were these derived of the current single crystal x-ray refinement, developed in the next Section.

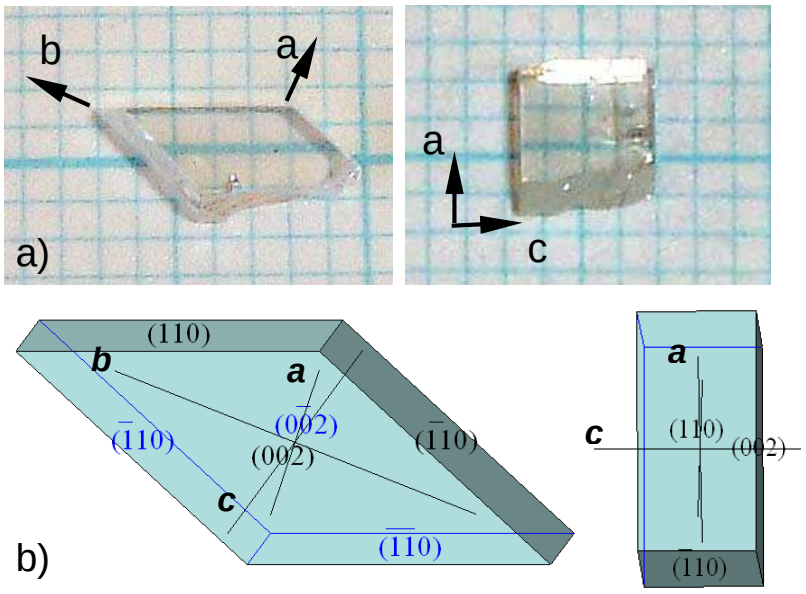

Figure 4. a) LiGdBaMo:Yb TSSG grown crystal: left) (001) oriented plate showing the spontaneously growth face; right) (010)-cut sample; b) Simulated morphology schemes of the crystal.

Crystalline structure

The single crystal X-ray determination of the structure of LiGdBaMo:Yb grown crystal has been performed in the monoclinic space group *C*2/*c* (No. 15), and the atomic coordinates considered initially were those reported previously.[12] Features of coordination polyhedra for cations in this description of the structure have been previously indicated

On the basis of the starting formula, our initial structure determination located Ba and Li fully occupying each one a different 4*e* site, Gd(Yb) and Li with occupancy factors (OF) fixed to 0.75:0.25 in one 8*f* site, and Mo1, Mo2 and the eight types of O in different 8*f* sites. The refinement yielded R_1 = 0.0723, with anisotropic displacement parameters for all atoms excepting Li in 4*e*, which was isotropically refined. In a next step we further refined the OF over 8*f* sites for Gd, Yb and Li cations, with the total population assumed to be 1. An improved R_1 = 0.044 was obtained with OF (Gd:Yb:Li) = 0.725(4):0.060(3):0.215(5), also with anisotropic thermal parameters for all atoms excepting Li in 4*e*. Details of this refinement are included in Table 2. Final crystallographic data, atomic coordinates and refined occupancy factors for Gd, Yb and Li simultaneously occupying the 8*f* crystal site appear in Table 3, and selected bonds are given in Table 4. A Table with anisotropic displacement parameters for all cations excepting Li(2), is also available in the Supporting Information. From these results the formula of the grown crystal should be written as $Li_{2.86}Gd_{2.90}Yb_{0.24}Ba_2(MoO_4)_8$.

Positions of peaks and their relative intensities in the XRPD profile generated using refined single crystal X-ray data agree with those of the prepared polycrystalline precursor, see Figure 5, which confirms the experimental procedure.

Thus, the cationic distribution achieved in the current refinement of the structure of LiGdBaMo:Yb corrects the previous one for this ternary molybdate host.[12] Our present results lead to the conclusion that Gd^{3+} occupies *only one* crystallographic site, 8*f*, and when Yb^{3+} replaces Gd^{3+} a disordered local environment around the first one exists as derived of the coexistence of Gd^{3+} and Li^{+} cations over this site.

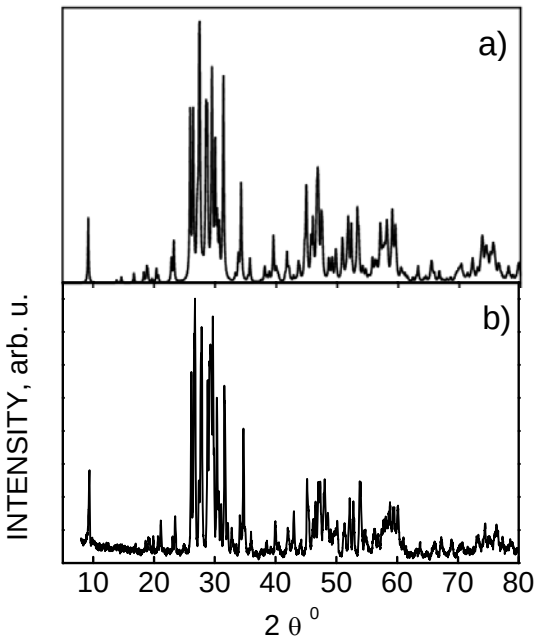

Figure 5. X-ray powder diffraction diagrams for: a) Calculated from single crystal X-ray data; b) Polycrystalline precursor LiGdBaMo:Yb

The crystalline structure is constituted by Gd(Yb)/LiO_8 distorted square antiprisms with symmetry C_1, distorted LiO_6 octahedra and BaO_{10} polyhedra, the two latter lying along the twofold *b* crystal axis, and two kinds of distorted MoO_4 tetrahedra, see Figure 6a. It can be envisaged in terms of layers perpendicular to the *c* axis formed by corrugated six-membered rings of Gd(Yb)/LiO_8 polyhedra, which are sharing edges, Figure 6b, left. Adjacent layers are connected through BaO_{10} polyhedra and LiO_6 octahedra, which are forming infinite planar layers, also constituted by shared-edge six-membered rings, with BaO_{10}-LiO_6 BaO_{10}- sequence, Figure 6b, right. The MoO_4 tetrahedra are linked to both sides of each layer through common vertices. This distinctive layered arrangement along the *c* axis is thus determining the observed shape of TSSG grown LiGdBaMo:Yb crystals.

Table 2. Crystal and Structure Refinement Data for $Li_{2.86}Gd_{2.90}Yb_{0.24}Ba_2(MoO_4)_8$

Formula weight	2062.93
Temperature (K)	296(2)
Wavelength (Å)	0.71073
Crystal system	Monoclinic
Space group	*C2/c* (No. 15)
Unit cell dimensions (Å)	a = 5.2355(3)
	b = 12.7396(8)
	c = 19.1626(11)
	β = 91.170(1)
Volume (Å^3)	1277.84(13)
Z	2
Calc. Density (g/cm^3)	5.319
Absorption coefficient (mm^{-1})	14.594
Absorption correction	SADABS
F(000)	1810
Crystal size (mm)	0.20 × 0.15 × 0.10
θ range for data collection (°)	3.20 to 29.23
Limiting indices	$-7 \le h \le 7$, $-17 \le k \le 17$; $-26 \le l \le 25$
Reflections collected	5653
Independent reflections	1582 (R_{int} = 0.0332)
Refinement method	Full-matrix least-squares on F^2
Data / restraints / parameters	1582 / 1 / 111
Goodness-of-fit on F^2	1.210
Final R indices [$I > 2\sigma(I)$]	R_1 = 0.0446, wR_2 = 0.1069
R indices (all data)	R_1 = 0.0524, wR_2 = 0.1127

Table 3. Atomic Coordinates ($\times 10^4$) and Equivalent Isotropic Displacement Parameters ($Å^2 \times 10^3$) for LiGdBaMo:Yb crystal

		x	*Y*	*Z*	OF [a]	U(eq) [b]
Li(1)	8*f*	10020(1)	1472(1)	4680(1)	0.215(5)	13 (1)
Gd(1)	8*f*	10020(1)	1472(1)	4680(1)	0.725(4)	13(1)
Yb(1)	8*f*	10020(1)	1472(1)	4680(1)	0.060(3)	13(1)
Ba	4*e*	10000	292(1)	2500		18 (1)
Li(2)	4*e*	5000	-1821(19)	2500		20 (5)
Mo(1)	8*f*	9913(2)	4403(1)	4074(1)		13 (1)
Mo(2)	8*f*	5011(2)	2387(1)	3494(1)		13 (1)
O(1)	8*f*	12534 (13)	4821 (6)	4631(4)		18 (1)
O(2)	8*f*	7657 (12)	5416 (5)	3949 (4)		16 (1)
O(3)	8*f*	7525(13)	1459(5)	3628(4)		18(1)
O(4)	8*f*	2717(14)	1994(5)	2870(4)		21(1)
O(5)	8*f*	3394(13)	2604(6)	4307(4)		19(1)
O(6)	8*f*	11259(13)	4137(6)	3272(4)		19(1)
O(7)	8*f*	6399(14)	3552(5)	3201(4)		20(1)
O(8)	8*f*	8468(14)	3314(6)	4522(4)		20(1)

Table 4. Selected Bond Lengths (Å) for LiGdBaMo:Yb

T(1)/Li(1)-O(1)#1 [a]	2.474(7)	Mo(1)-O(1)	1.802(7)
T(1)/Li(1)-O(1)#8	2.454(7)	Mo(1)-O(2)	1.763(7)
T(1)/Li(1)-O(2)	2.400(7)	Mo(1)-O(6)	1.739(7)
T(1)/Li(1)-O(3)	2.379(7)	Mo(1)-O(8)	1.806(7)
T(1)/Li(1)-O(5)#6	2.401(7)		
T(1)/Li(1)-O(5)#7	2.404(7)	Mo(2)-O(3)	1.784(7)
T(1)/Li(1)-O(8)	2.500(7)	Mo(2)-O(4)	1.751(7)
T(1)/Li(1)-O(8)#7	2.421(7)	Mo(2)-O(5)	1.809(7)
		Mo(2)-O(7)	1.750(7)
Li(2)-O(4)#3	2.183(19)		
Li(2)-O(4)#4	2.183(19)	T(1)/Li(1)-T(1)/Li(1)#7	3.9320(11)
Li(2)-O(6)#1	2.017(17)	T(1)/Li(1)-T(1)/Li(1)#8	3.8707(11)
Li(2)-O(6)#2	2.017(17)		
Li(2)-O(7)#1	2.358(9)	Ba-Li(2)	3.755(18)
Li(2)-O(7)#2	2.358(9)	Ba#1-Li(2)	3.68(2)
Ba-O(2)#2	3.083(7)	Ba- T(1)/Li(1)	4.4395(11)
Ba-O(2)#4	3.083(7)		
Ba-O(3)	2.946(7)	T(1)/Li(1)#7-Mo(1)	3.7230(9)
Ba-O(3)#11	2.946(7)	T(1)/Li(1)#8-Mo(1)	3.7042(10)
Ba-O(4)#6	2.681(7)	T(1)/Li(1)#5-Mo(2)	3.6870(9)
Ba-O(4)#9	2.681(7)	T(1)/Li(1)#7-Mo(2)	3.7892(10)
Ba-O(6)#1	2.882(7)		
Ba-O(6)#10	2.882(7)	Li(2)-Mo(1)	3.365(7)
Ba-O(7)#2	2.685(7)	Li(2)-Mo(1)	3.397(7)
Ba-O(7)#4	2.685(7)	Li(2)-Mo(2)	3.416(7)
		Li(2)-Mo(2)	3.366(7)

[a] T indicates Gd and Yb

Symmetry transformations used to generate equivalent atoms:

#1 x-1/2,y-1/2,z #2 -x+3/2,y-1/2,-z+1/2 #3 -x+1/2,y-1/2,-z+1/2

#4 x+1/2,y-1/2,z #5 x-1,y,z #6 x+1,y,z #7 -x+3/2,-y+1/2,-z+1

#8 -x+5/2,-y+1/2,-z+1 #9 -x+1,y,-z+1/2 #10 -x+5/2,y-1/2,-z+1/2

#11 -x+2,y,-z+1/2 #12 x+1/2,y+1/2,z #13 x-1/2,y+1/2,z

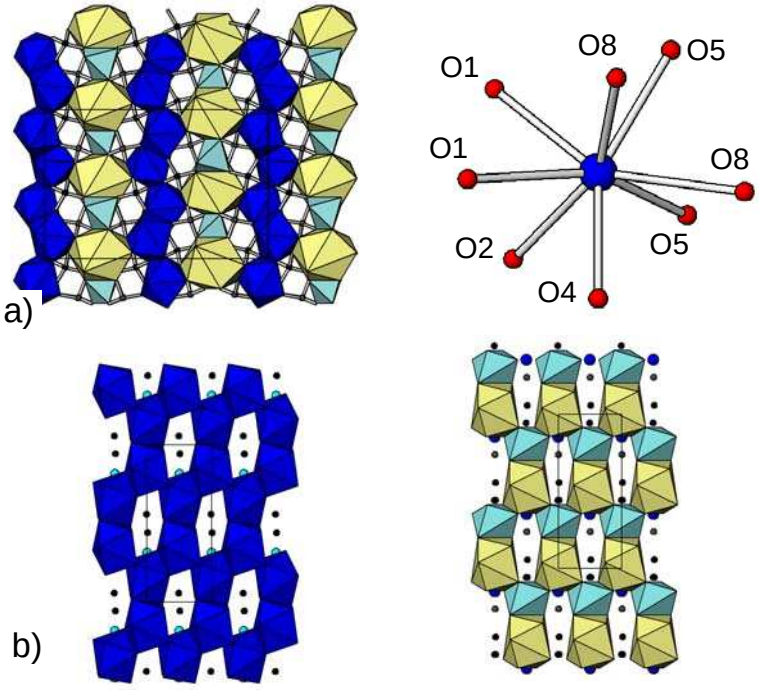

Figure 6. Structure of LiGdBaMo:Yb crystal: a) left, *bc* plane view showing Gd(Yb)/LiO_8 distorted square antiprisms (blue), LiO_6 distorted octahedra (cyan) and BaO_{10} polyhedra (yellow); right, the C_1 Gd(Yb)/LiO_8 coordination polyhedron; b) left, *ab* plane of six-membered rings (6R) of Gd(Yb)/LiO_8; right, adjacent *ab* plane of 6R LiO_6 and BaO_{10}.

This structure can be considered as derived of the Li-insertion in vacant 4*e* positions in the isostructural $Gd_2Ba(MoO_4)_4$,[26] as can be seen in Figure 7. These empty sites, aligned along the *b*-axis between BaO_{10} polyhedra, suppose cavities limited by six oxygen vertices that provide the octahedral environment around Li cations. Similar Li-insertion can be viewed in isostructural *C*2/*c* $LiRbBi_2(MoO_4)_4$,[36] and in Li-doped triclinic α-$KDy(MoO_4)_2$.[37]

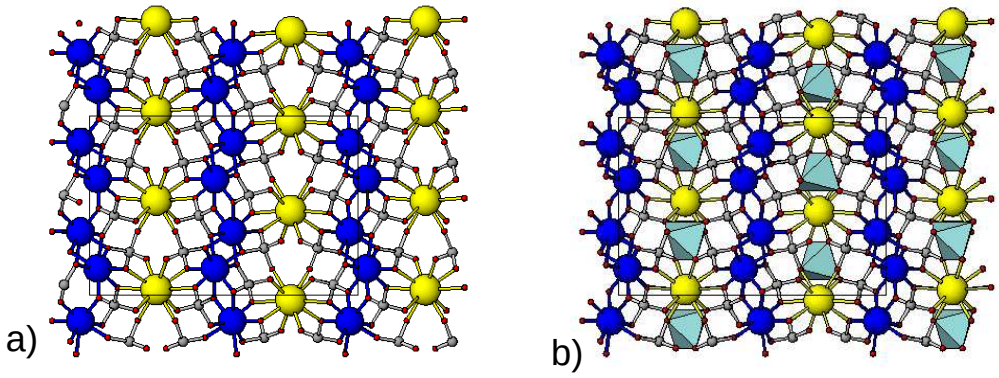

Figure 7 a) View of the *bc* plane of the monoclinic *C*2/*c* $Gd_2Ba(MoO_4)_4$ structure; b) view of the *bc* plane of isostructural LiGdBaMo:Yb showing the insertion of LiO_6 in octahedral cavities between BaO_{10} polyhedra along the *b* axis.

Taking in consideration the characteristics of the structure of the LiGdBaMo:Yb crystal, i.e., $\beta \approx 90^0$ and its layered nature perpendicular to the *c*-direction, as well as the SHAPE[16] simulations of the growth habit, we can establish that the largest face of the TSSG grown crystals are perpendicular to the *c*-axis. The comparison of experimentally obtained Laue patterns with those simulated [20] from the unit cell dimensions and symmetry of the crystal allowed to identify the direction of orthogonal *a* and *b* axes in the grown crystal, in the way that has been indicated in the Figure 4a.

In this monoclinic and thus biaxial crystal one of the principal optical axes is parallel to the unique twofold axis of the crystal, and the two other lie in a perpendicular plane to this axis. But since the preparation of adequate prisms for precise measurements of refractive indices is problematical due to the cleavable nature of the crystal, for the description of the polarization characteristics we can consider that its almost orthorhombic nature would suppose the two other optic axes practically aligned with the two remaining crystallographic axes. Hence, just for convenience of description the three optical axes will be arbitrarily named by collinearity with the determined crystallographic axes. Spectra measurements have been thus performed in configurations E//*a*, E//*b* and E//*c*. After polishing the as-

grown crystal was used to measure the E/*a*, E//*b* spectra, while for E//*c* measurements a polished *b*-cut sample (see Figure 4a-right), from another TSSG crystal with the same characteristics, was used.

Spectroscopic Characterization

Figure 8 shows the transparency range of the LiGdBaMo:Yb crystal at room temperature and at 6 K. The absorption edge was determined from optical absorption (OA) measurements in the ultraviolet, through the linear extrapolation to zero of the stepping absorption, in each case. Whereas at 300 K E//*a* and E//*c* OA spectra show less than 1 nm difference, 348.0 and 347.6 nm, respectively, and narrow UV transparency for the E//*b* spectrum, 351.3 nm, at 6 K the three polarizations present different and extended transparencies, 335.0, 337.0 and 333.1 nm for E//*a*, E//*b* and E//*c*, respectively. The IR window extends up to the onset of multiphonon absorption, near 3.7 μm, related to MoO_4 vibrations.[38] It is worth to noting that LiGdBaMo has similar or larger bandgap than previously studied tetragonal double molybdate femtosecond laser crystal hosts.[8, 39, 40]

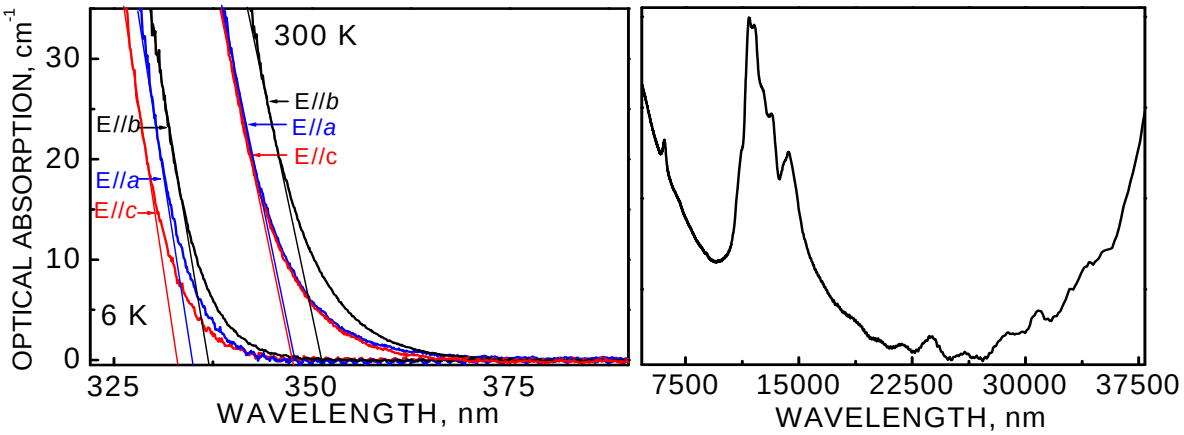

Figure 8. Optical absorption at 6 K and 300 K of LiGdBaMo:Yb single crystal. The straight lines in the polarized spectra at the UV limit are used to determine the effective bandgaps. For 300 K unpolarized IR spectrum the absorption scale is arbitrary.

For the description of energy levels of the $4f^{13}$ configuration of Yb^{3+} in LiGdBaMo the low temperature (6 K) (OA) and the photoluminescence (PL) spectra have been measured. The C_1 local symmetry of the single 8*f* site of Yb^{3+} in LiGdBaMo is expected to split the two multiplets $^2F_{7/2}$ (n) and $^2F_{5/2}$ (n') into four (n = 0, 1, 2, 3), and three (n' = 0',1',2') doubly degenerate Stark levels, respectively, all of them with irreducible representation Γ_1. For this point symmetry no selection rules for E//*a*, E//*b* and E//*c* polarizations exist, that is, all electric-dipole ED or magnetic-dipole MD transitions are allowed. Figure 9 shows the polarized 6 K OA spectra corresponding to $^2F_{7/2}$ (0) → $^2F_{5/2}$ (n') transitions (shortly 0 → n') and the PL spectra for $^2F_{5/2}$(0')→ $^2F_{7/2}$ (n) (shortly 0' → n) transitions. It can be seen that although the observed peaks are the same in the three polarizations, the anisotropy for such biaxial crystal is important, with clearly large OA for E//*a* and E//*b* spectra. The presence of a unique zero line absorption, 0 ↔ 0', agrees with the existence of a single 8*f* site for Yb^{3+} ions in the LiGdBaMo crystal structure. However, even if this line is the sharpest one in OA spectra, its observed FWHM is ~ 19 cm^{-1}. For comparison, the FWHM of the same transition in the ordered monoclinic Yb-$KY(WO_4)_2$ is ~ 10 cm^{-1}.[41] This broadening is attributed to the structural short-range cationic disorder derived of Yb^{3+} substitution over the shared crystal site, which creates a distribution of slightly different crystal fields around Yb^{3+} centers.

Despite its simplicity, the proclivity of the $4f^{13}$ electronic structure of Yb^{3+} to interact with lattice vibrations[5] makes difficult the identification of some of its energy levels. While transitions observed in 6 K OA spectra at 10248 cm^{-1} and 10413 cm^{-1} can be straightforwardly assigned to 0 → 0' and 0 → 1' transitions, it is difficult to ascertain the energy of the 0→2' in the complex 10550-10700 cm^{-1} observed region, which must correspond to its mixture with vibronic sidebands. The observed bands in 6 K PL spectra, which correspond to 0'→ n transitions, also show some structure. Thus, for the confident identification of Yb^{3+} energy levels the interpretation of the 6 K spectra needs an assessment through predictive methods of crystal field (CF) interactions. The widely tested semi-empirical CF Simple Overlap Model SOM,[42] which considers the structural characteristics of the first coordination shell around Yb^{3+},[9, 43] has been used here to derive a proper set of CF parameters accounting for the CF

potential of Yb^{3+} in the LiGdBaMo crystal. Crystallographic data are these from the previous X ray analysis, and the effective charge for oxygen and the magnitude of the overlap integral ρ between Yb^{3+} and oxygen wavefunctions, have been taken as –1.2, and 0.08, respectively.[42] Using SOM predicted CF parameters the simulation of the sequence of energy levels was performed with a previously developed code.[44,45] It requires only two free-ion (FI) parameters, E_0 and the spin-orbit coupling constant ζ, whose variation with the crystal host is theoretically weak, and consequently can be reasonably adapted from previous values in the literature.[9] Used FI and SOM CF parameters and the resulting simulated sequence of Yb^{3+} energy levels are summarized in Table 5. The agreement between the SOM calculated total splitting for $^2F_{7/2}$ (462 cm^{-1}) and the experimental energy difference between the first and the last peaks observed in the PL spectra (460 cm^{-1}), as well as for the energy positions of the bands of 0 → 0' and 0 → 1' transitions, confirms the reliability of the method, and allow us to ascribe the peak observed in OA spectra at 10634 cm^{-1} to the 0 → 2' transition. The peak at 10687 cm^{-1} in the same OA spectra would likely correspond to the coupling with a phonon of energy of ~53 cm^{-1}. Thus, it is reasonable to considerer phenomenological splitting schemes of 0, 223, 353 and 460 cm^{-1}, for the $^2F_{7/2}$ ground multiplet, and 10248, 10413 and 10634 cm^{-1} for the $^2F_{5/2}$ excited multiplet of Yb^{3+} in LiGdBaMo. Moreover, their barycentres at 259 cm^{-1} and 10432 cm^{-1} are consistent the relationship describing the "barycentre law" developed for Yb^{3+}.[6]

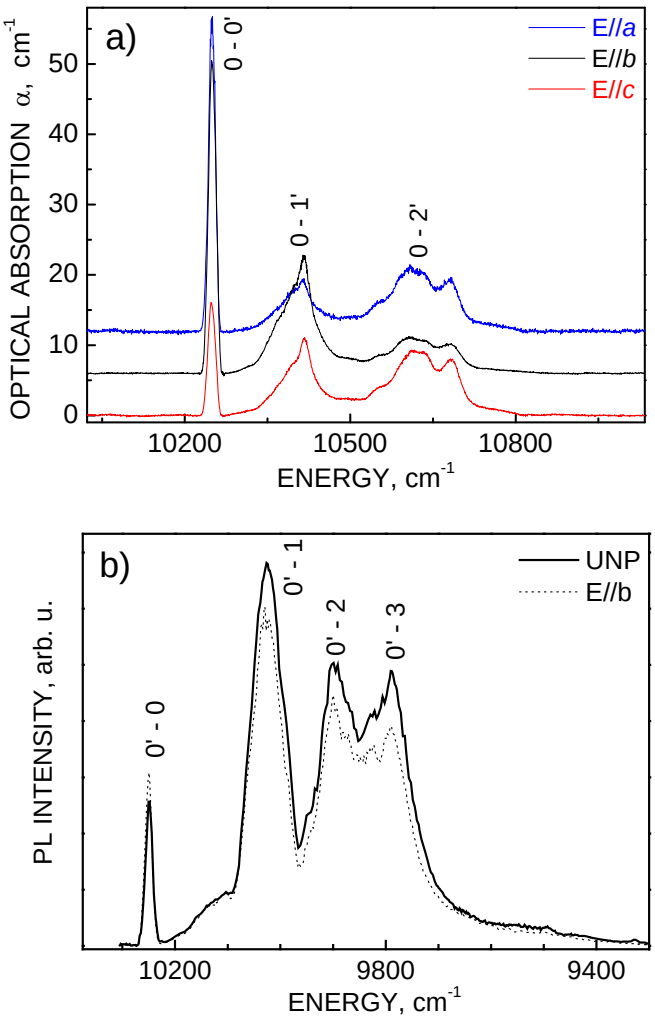

Figure 9. a) 6 K absorption coefficient of LiGdBaMo:Yb crystal in the three polarizations (for sake of clarity the *y*-axis has been displaced); b) 6 K photoluminescence excited at λ_{EXC} = 960 nm, unpolarized and along the main polarization direction

Table 5. Free ion (E^0 and ζ) and SOM Crystal Field (B_q^k,S_q^k) Parameters (cm^{-1}) [a] Used to Calculate the Energy Levels (italics) for Yb^{3+} (8*f* site) in LiGdBaMo crystal. The Experimental Energy Levels Appear at the Right Side in the Column.

E^0, ζ	4628.04, 2901.60
B_0^2, B_2^2	168, 88
B_0^4, B_2^4, S_2^4, B_4^4, S_4^4	-234, -401, -25, -589, -725
B_0^6, B_2^6, S_2^6, B_4^6, S_4^6, B_6^6, S_6^6	-34, -199, -241, -22, -150, -140, -201
$^2F_{5/2}(2')$	*10628* – 10634
$^2F_{5/2}(1')$	*10422* – 10413
$^2F_{5/2}(0')$	*10250* – 10248
$^2F_{7/2}(3)$	*462* – 460
$^2F_{7/2}(2)$	*392* – 353
$^2F_{7/2}(1)$	*243* – 223
$^2F_{7/2}(0)$	*0* – 0

[a] The value for the overlap integral ρ between Yb^{3+} and oxygen orbital wavefunctions is taken as 0.08, and the effective charge for oxygens as –1.2. [42]

Conclusions

The monoclinic (space group *C*2/*c*) LiGdBaMo:Yb crystal has been successfully grown with optical quality by the TSSG method. The crystal structure has a single 8*f* site occupied simultaneously by Gd^{3+} (72.5%), Yb^{3+} (6%) and Li^+ (21.5%). This leads to a locally disordered environment around Yb^{3+} ions, which generates the observed inhomogeneous broadening of the spectral features. From experimental spectroscopic results it is clear that the CF splitting for the $^2F_{7/2}$ Yb^{3+} ground multiplet is not so large as thought initially. It is explained by the absence of the second 4*e* site for Gd^{3+}(Yb^{3+}) site in the crystal structure of LiGdBaMo, which would have produced the strongest CF effect on Yb^{3+} energy levels. However, this splitting remains similar to those observed for Yb^{3+} in tetragonal $NaT(WO_4)_2$ T = Y,[2]

Gd,[9] or Lu,[10] and in Yb-$LiGd(MoO_4)_2$,[8] all of them tunable lasers. Furthermore, the higher anisotropy of OA and PL polarized spectra would be responsible for absorption and emission cross-sections for specific crystal orientations of LiGdBaMo:Yb higher than in the above mentioned tetragonal laser crystals.[46] On the other hand, the combination of disordered cationic environments around Yb^{3+}, with its electron-phonon coupling can explain the observed tunability of 33 nm at the threshold of the laser oscillation in LiGdBaMo:Yb crystal.[46]

Acknowledgments

This work was supported by projects MAT2005-6354-C03-01 and MAT2008-06720-C02-01, Spain. A.G-C additionally acknowledges his FPU2003-3018 Spanish grant.

Supporting Information Available

Crystallographic information file of LiGdBaMo:Yb crystal; an additional Table with anisotropic displacement parameters; Room temperature optical absorption spectra of two samples of LiGdBaMo:Yb synthesized at 560 ^{0}C and at 850 ^{0}C. This material is free of charge via the internet at http:// pubs.acs.org.

References

[1] Zaouter, Y.; Didierjean, J.; Balembois, F.; Leclin, G. L.; Druon, F.; Georges, P.; Petit, J.; Goldner, P.; and Viana, B. *Opt. Lett*. **2006**, 31, 119.

[2] García-Cortés, A.; Cano-Torres, J.M.; Serrano, M.D.; Cascales, C.; Zaldo, C.; Rivier, S.; Mateos, X.; Griebner U.; and Petrov, V. *IEEE J. Quant. Electron*. **2007**, 43, 758.

[3] Giesen, A.; Hügel, H.; Voss, A.; Wittig, K.; Brauch, U.; Opower, H. *Appl. Phys. B* **1994,** 58, 363.

[4] Liu, J.; Petrov, V.; Mateos, X.; Zhang, H.; and Wang, J. *Opt. Lett*. **2007**, 32, 2016.

[5] Ellens, A. ; Andres, H. ; Meijerink, A. ; Blasse, G. *Phys. Rev. B* **1997**, 55, 173; Ellens, A.; Andres, H.; ter Heerdt, M.L. H.; Wegh, R.T.; Meijerink, A.; Blasse, G. *Phys. Rev. B* **1997**, 55, 180.

[6] Haumesser, P.H.; Gaumé, R.; Viana B.; Antic-Fidancev, E.; and Vivien, D. *J. Phys.: Condens. Matter* **2001**, 13, 5427.

[7] Druon, F.; Balembois, F.; and Georges, P. *Opt. Exp*ress **2004**, 12, 5005.

[8] Rico, M.; Griebner, U.; Petrov, V.; Ortega, P.; Xiumei, H.; Cascales C.; and Zaldo, C. *J. Opt. Soc. Am.* B **2006**, 23, 1083.

[9] Cascales C.; Serrano, M.D.; Esteban-Betegon, F.; Zaldo, C.; Peters, R.; Johannsen, J.; Mond, M.; Peterman, K.; Huber, G.; Ackermann, L.; Rytz, D.; Dupré, C.; Rico, M.; Griebner, U.; Petrov, V. *Phys. Rev. B*, **2006**, 17, 174114.

[10] García Cortés, A.; Han, X.; Cano-Torres, J.M.; Cascales, C.; Zaldo, C.; Mateos, X.; Petrov V.; and Valle, F.J. *J. Appl. Phys.* **2007**, 101, 063110.

[11] Inorganic Crystal Structure Database ICSD, Fachinformationszentrum-Karlsruhe, Germany, 2006.

[12] Kletsova, R.F.; Vasil'ev, A.D.; Glinskaya, L.A.; Kruglik, A.I.; Kozhevnikova N.M.; and Korsun, V.P. *J. Struct. Chem*. **1992**, 33, 443. [Translated from *Zhur. Struk. Khimii*, **1992**, 33, 126].

[13] Shannon, R.D.; Gummerman, P.S.; Chenavas, J. *J. Am. Miner*. **1975**, 60, 714.

[14]A.A. Kaminskii, *Crystalline Lasers: Physical Properties & Operating Schemes.* CRC Press: Boca Raton, FL, **1996**.

[15]Batay, L.E.; Demidovich, A.A.; Kuzmin, A.N.; Ryabtsev, G.I.; Stręk, W.; and Titov, A.N. *Spectrochim. Acta A* **1998**, 54, 2117.

[16] Dowty, E. *SHAPE for Windows*, Software for drawing crystal shapes, v.7.2.1, **2006**.

[17] International Tables for Crystallography; Kynoch Press: Birmingham, United Kingdom, 1974; Vol. 4.

[18] *SHELXTL Version 6.10 software package;* Siemens Energy and Automation Inc. Analytical Instrumentation.

[19] Dowty, E. *ATOMS* v. 5.1, Computer Program for Displaying Atomic Structures, Kingsport, TN, 2001.

[20] Marín and Dieguéz, E. *LAUE Software*, in *Orientation of Single Crystals by Back-Reflection Laue Pattern*; World Scientific: Singapore, 1999.

[21] Rico, M.; Liu, J.; Griebner, U.; Petrov, V.; Serrano, M.D.; Estebán-Betegón, F.; Cascales, C.; Zaldo, C. *Opt Express* **2004**, *12*, 5362.

[22] Liu, J.; Cano-Torres, J.M.; Estebán-Betegón, F.; Serrano, M.D.; Cascales, C.; Zaldo, C.; Rico, R.; Griebner, U.; Petrov, V. *Opt. Laser Technol.* **2007**, *39*, 558.

[23] Liu, J.; Cano-Torres, J.M.; Cascales, C.; Estebán-Betegón, F.; Serrano, M.D.; Volkov, V.; Zaldo, C.; Rico, R.; Griebner, U.; Petrov, V. *Phys. Stat. Sol. (a)* **2005**, *202(4)*, R29.

[24] Rico, M.; Liu, J.; Cano-Torres, J.M.; García-Cortés, A.; Cascales, C.; Zaldo, C.; Griebner, U.; Petrov, V. *Appl. Phys. B*, **2005**, *81*, 621.

[25] JCPDS-ICDD card file 77-0830 for $Li_3Gd_3Ba_2(MoO_4)_8$, Swarthmore, PA, USA.

[26] Kiseleva, I.I.; Sirota, M.I.; Ozerov, R.I.; Balakireva, T.P.; Maier, A.A. *Kristallografiya* **1979**, 24, 1277.

[27] JCPDS-ICDD card file 36-0192 for $Gd_2Ba(MoO_4)_4$, Swarthmore, PA, USA.

[28] Haomiau Zhu, Yujin Chen, Yanfu Lin, Xinghong Gong, Qiguang Tan, Zundu Luo, Yindong Huang, *J. Appl. Phys*. **2007**, 101, 063109.

[29] Tomaszewski, P.E. *Phase Transitions,* **1992**, 38, 127.

[30] Colón, C.; Alonso Medina, A.; Fernández, F.; Sáez Puche, R.; Volkov, V.; Cascales, C.; and Zaldo, C. *Chem. Mater*. **2005**, 17, 6635.

[31] Allan D.R.; and Nelmes, R.J. *J. Phys.:Condens. Matter* **1992**, 4, L395.

[32]Radaelli, P.G.; Cox, D.E.; Marezio M.; and Cheong, S-W. *Phy. Rev*. B **1997**, 55, 3015.

[33] Friese, K.; Kanke, Y.; Fitch, A.N.; Grzechnik, A. *Chem. Mater*. **2007**, 19, 4882.

[34] McCaroll W. H;. and Greenblatt, M. *J. Sol. State Chem.* **1984**, 54, 282.

[35] Dowty, E. *Am. Miner*. 1980, 65, 465.

[36] Kletsova, R.F.; Glinskaya, L.A.; Alekseev, V.I.; Khalbaeva, K.M.; and Khaikina, E.G. *J. Struct. Chem.* **1993**, 34, 789. [Translated from *Z. Struk. Khimii*, **1993**, 34, 152].

[37] Basovich, O.M.; Khaikina, E.G.; Solodovnikov, S.F.; and Tsyrenova, G.D. *J. Sol. State Chem.* **2005**, 178, 580.

[38] Hanuza, J.; Maczka, M.; Hermanowicz, K.; Dereń, P.J.; Stręk, W.; Folcik L.; and Drulis, H. *J. Sol. State Chem.* **1999**, 148, 468.

[39] Volkov, V.; Cascales, C.; Kling A.; and Zaldo, C. *Chem. Mat.* **2005,** 17, 291.

[40] Rico, M.; Méndez-Blas, A.; Volkov, V.; Monge, M.A.; Cascales, C.; Kling, A.; Fernández-Díaz, M.T.; and Zaldo, C. *J. Opt. Soc. Am. B* **2006**, 23, 2066.

[41] Kuleshov, N.V.; Lagatsky, A. A.; Podlipensky, A.V.; Mikhailov, V.P.; Huber, G. *Opt. Lett*. **1997**, 22, 1317.

[42] P. Porcher P, M. Couto dos Santos M and O. Malta O, *Phys. Chem. Chem. Phys.* **1999**, *1*, 397.

[43] C. Cascales, R. Sáez-Puche and C. Zaldo, *Chem. Phys.* **1999**, *240*, 291.

[44] Cascales, C.; Antic-Fidancev, E.; Lemaitre-Blaise, M.; and Porcher, P. *J. Phys.: Condens. Matter* **1992**, *4*, 2721.

[45] Cascales, C.; Sáez Puche, R.; and Porcher, P. *J. Sol. State Chem.* **1995**, *114*, 52.

[46] García-Cortés, A.; Zaldo, C.; Cascales, C.; Mateos, X.; Petrov, V. *Opt. Express*. **2007**, *15*, 18162.